



Article

Study on Apparent Permeability Model for Gas Transport in Shale Inorganic Nanopores

Shuda Zhao ¹, Hongji Liu ², Enyuan Jiang ³, Nan Zhao ⁴, Chaohua Guo ² and Baojun Bai ^{1,*}¹ GGPE, Missouri University of Science and Technology, Rolla, MO 65401, USA² Key Laboratory of Theory and Technology of Petroleum Exploration and Development, China University of Geosciences, Wuhan 430074, China³ China National Oil and Gas Exploration and Development Co. Ltd., (CNOOC), Beijing 100034, China⁴ SINOPEC Henan Oilfield Company, Nanyang 473132, China

* Correspondence: Baib@mst.edu

Abstract: Inorganic nanopores occurring in the shale matrix have strong hydrophilicity and irreducible water (IW) film can be formed on the inner surface of the pores making gas flow mechanisms in the pores more complex. In this paper, the existence of irreducible water (IW) in inorganic pores is considered, and, based on the Knudsen number (K_n) correction in shale pores, a shale gas apparent permeability model of inorganic nano-pores is established. The effect of the K_n correction on the apparent permeability, the ratio of flow with pore radius and the effect of IW on the apparent permeability are assessed. The main conclusions are as follows: (1) at low pressure (less than 10 MPa) and for medium pore size (pore radius range of 10 nm–60 nm), the effect of the K_n correction should be considered; (2) considering the effect of the K_n correction, bulk phase transport replaces surface diffusion more slowly; considering the existence of IW, bulk phase transport replaces surface diffusion more slowly; (3) with increase in pressure, the IW effect on gas apparent permeability decreases. Under low pressure, the IW, where pore size is small, promotes fluid flow, while the IW in the large pores hinders fluid flow. In conditions of ultra-high pressure, the IW promotes gas flow.



Citation: Zhao, S.; Liu, H.; Jiang, E.; Zhao, N.; Guo, C.; Bai, B. Study on Apparent Permeability Model for Gas Transport in Shale Inorganic Nanopores. *Energies* **2022**, *15*, 6301. <https://doi.org/10.3390/en15176301>

Academic Editor: Hossein Hamidi

Received: 9 August 2022

Accepted: 27 August 2022

Published: 29 August 2022

Publisher's Note: MDPI stays neutral with regard to jurisdictional claims in published maps and institutional affiliations.



Copyright: © 2022 by the authors. Licensee MDPI, Basel, Switzerland. This article is an open access article distributed under the terms and conditions of the Creative Commons Attribution (CC BY) license (<https://creativecommons.org/licenses/by/4.0/>).

Keywords: shale gas; inorganic nanopore; apparent permeability; irreducible water; percolation mechanism; Knudsen number correction

1. Introduction

The world is facing serious environmental problems and energy shortages [1–3]. Countries around the world have gradually turned their attention to shale gas. A shale gas reservoir is an unconventional reservoir that integrates production, storage and accumulation [4–11]. The shale pore structure is very complex with a pore size in the nanometer range, and is very different from the pore structure of a conventional gas reservoir [12–17]. The complex pore structure determines the complex and variable storage status of shale gas and indirectly affects its production [18].

Beskok and Karniadakis [19] derived the Hagen–Poiseuille equation applicable at the nanometer scale and introduced a rare effect coefficient to the model. Javadpour [20] characterized the micro-migration characteristics of gas, establishing a gas mass flow equation similar to Darcy's formula, and first formally proposed the concept of apparent permeability. Civan [21] proposed a model for calculating apparent shale permeability using the Beskok–Karniadakis model, which considers the effects of curvature, inherent permeability, the gas slippage coefficient, porosity, and the rare effect coefficient on the gas flow. In this model, the parameters are relatively easy to obtain, so researchers often cite them. Xiong et al. [22] considered surface diffusion, studied the desorption of gas, and introduced a correction coefficient into the model showing that the gas mass flux was not represented by simple addition. For the first time, these authors proposed an apparent permeability model for shale gas transport which combined multiple mechanisms: surface diffusion,

Knudsen diffusion and viscous flow. Dababi et al. [23] extended the single circular tube nanopore Javadpour model to porous media and introduced the fractal dimension into Knudsen diffusion to address the influence of different pore surface roughness. Li et al. [24] studied the irreducible water (IW) in inorganic shale pores and established a gas transport model that considered the distribution of bound water in inorganic pores. Wu et al. [25] established a relatively complete apparent permeability model extending different properties of apparent permeability, which considers the real gas effect, the shale pore structure, the shale rock stress sensitivity and the matrix shrinkage effect. Wang et al. [26] introduced monolayer and multilayer adsorption models involving a variety of percolation mechanisms and developed a real gas flow model in organic shale pores.

However, there has been little research on the influence of water in shale pores on gas flow. In this paper, a shale gas apparent permeability model, considering the effect of irreducible water, is proposed. A correction of the Knudsen number in porous media is also considered. The influence of the Knudsen number correction is examined by comparing whether the Knudsen number correction is considered or not. The influence of irreducible water in pores on gas flow is analyzed by comparing whether the IW effect in pores is considered or not.

2. Establishment of Apparent Permeability Model

2.1. Assumptions

1. The composition of shale gas is considered to be methane only;
2. The occurrence of shale gas involves the coexistence of a free state and an adsorption state;
3. The change in pore radius caused by the presence of gas is considered;
4. Of the water molecules in the inorganic pores of shale gas, only irreducible water is considered—mobile water molecules are not considered;
5. The influence of stress on shale is not considered.

2.2. The Process of Permeability Model Establishment

Figure 1 represents the core idea of the paper and establishment of the mathematical model.

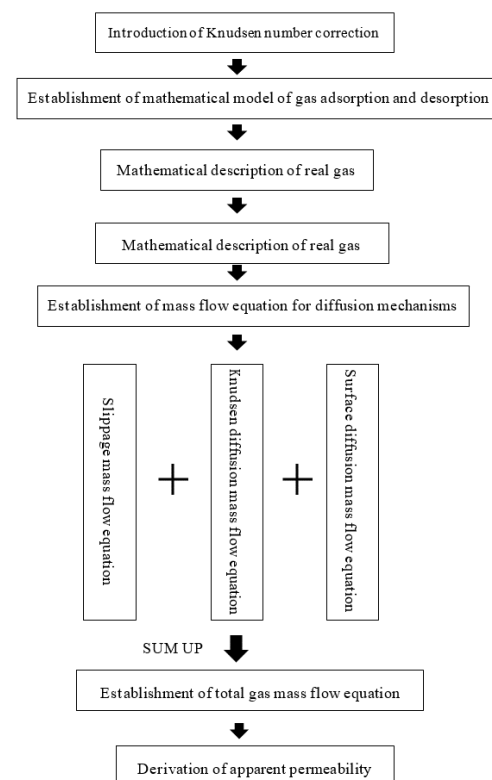


Figure 1. Flowchart of permeability model establishment.

2.3. Derivation of Gas Flow Equation

The Knudsen number in free space is generally calculated as follows [27]:

$$K_n = \frac{1}{2\sqrt{2}\pi N_g d^2 r} \quad (1)$$

where,

$$N_g = \frac{P}{k_b T} \quad (2)$$

N_g is the molecular density, m^3 ; d is the molecular diameter, m ; k_b is the Boltzmann constant, 1.38×10^{-23} J/K; r is the pore radius, m ; and P is the gas pressure, Pa.

In porous media, calculating the Knudsen number involves consideration of the inter-molecular collisions and interactions with the media to produce additional collisions [28]. The Knudsen number in porous media can be expressed as:

$$K_{np} = \frac{\lambda_m}{2r_e} = \frac{1}{\left(2\sqrt{2}\pi N_g d^2 + \frac{\zeta S_r \rho_r}{2\phi}\right) r_e} \quad (3)$$

where, S_r is the shale specific surface area, m^2/g ; ρ_r is the shale density, kg/m^3 ; ϕ is the porosity, dimensionless; and ζ is the equation coefficient, 1000.

In inorganic shale, the existence of water film should be considered. The three-phase adsorption and desorption model is used to calculate the gas adsorption volume [29]:

$$V = \beta \frac{V_H P}{P + P_H} + (1 - \beta) \frac{V_L P}{P + P_L} \quad (4)$$

where, V is the gas adsorption volume, m^3/kg ; V_L is the Langmuir saturated adsorption volume, m^3/kg ; P_L is the Langmuir pressure constant, Pa; V_H is the liquid-gas Langmuir adsorption volume, m^3/kg ; P_H is the liquid-gas pressure constant, Pa; and β is the coverage of water molecules. The definition is as follows:

$$\beta = \frac{A_H}{A_{total}} \quad (5)$$

where, A_{total} is the total surface area of shale pores, m^2 ; and A_H is the surface area wetted by water molecules, m^2 .

The total surface coverage of adsorbed gas in the three phase adsorption model is:

$$\theta = \frac{(1 - \beta)P}{P + P_L} + \frac{\beta P}{P + P_H} \quad (6)$$

In inorganic pores, the shale matrix pore radius is modified by the three-phase adsorption and desorption model as follows [30]:

$$r_e = r_m - d_H \beta - d \left[\frac{(1 - \beta)P}{P + P_L} + \frac{\beta P}{P + P_H} \right] \quad (7)$$

where, r_e is the real pore radius, m ; d_H is the diameter of water molecules, m ; d is the diameter of methane molecules, m ; and r_m is the pore radius without fillers, m . Considering the real gas, the gas compression factor is as follows [31,32]:

$$Z = 0.702P_r^2 e^{-2.5T_r} - 5.524P_r e^{-2.5T_r} + 0.044T_r^2 - 0.164T_r + 1.15 \quad (8)$$

$$P_r = P/P_c \quad (9)$$

$$T_r = T/T_c$$

where, P_r is the methane converted pressure, dimensionless; P_c is the methane critical pressure, Pa; T_r is the methane converted temperature, dimensionless; and T_c is the methane critical temperature, K. The equation for the equation for slippage mass flow with K_n is as follows [33]:

$$F_v = -\frac{\rho r_e^2}{8\mu} (1 + \alpha \cdot K_n^*) \left(1 + \frac{4K_n^*}{1 - b \cdot K_n^*} \right) \nabla P \quad (10)$$

where, F_v is the slippage mass flow, kg/ (m²·s); μ is the methane viscosity, Pa·s; ρ is the gas density, kg/m³; and α is the fitting function about K_n . The expression is as follows [34]:

$$\alpha = \alpha_0 \tan^{-1} \left(4 \cdot K_n^{*0.4} \right) \quad (11)$$

where, α_0 and β are fitting constants, dimensionless. Then the velocity form of the slippage flow is:

$$v_v = -\frac{r_e^2}{8\mu} (1 + \alpha \cdot K_{np}) \left(1 + \frac{4K_{np}}{1 - bK_{np}} \right) \nabla P \quad (12)$$

The Knudsen diffusion mass flow is as follows [35]:

$$F_k = -MD_k \nabla c = -\frac{MD_k}{ZRT} \nabla P \quad (13)$$

where, F_k is the Knudsen diffusion mass flow, kg/ (m²·s); M is the molar mass of methane, kg/mol; and D_k is the Knudsen diffusion coefficient, m²·s, which is given by the following equation:

$$D_k = \frac{2r_e}{3} \sqrt{\frac{8RT}{\pi M}} \quad (14)$$

Its flow velocity is:

$$v_k = -\frac{D_k}{P} \nabla P \quad (15)$$

The coefficient correction of the bulk phase transport mechanism is as follows [34]:

$$\begin{aligned} \varepsilon_v &= \frac{1}{1 + K_n^*} \\ \varepsilon_k &= \frac{1}{1 + 1/K_n^*} \end{aligned} \quad (16)$$

Then the surface diffusion mass flow is as follows [36]:

$$F_s = -\frac{D_s C_s}{P} \nabla P \quad (17)$$

where, D_s is the gas surface diffusion coefficient, m²/s; and C_s is the adsorption capacity of methane, kg/m³, which is as follows:

$$C_s = \frac{4M\theta}{\pi d^3 N_A} \quad (18)$$

The surface diffusion coefficient is given as follows [37]:

$$D_s = D_{s0} \frac{(1 - \theta) + \frac{\kappa}{2}\theta(2 - \theta) + [H(1 - \kappa)](1 - \kappa)\frac{\kappa}{2}\theta^2}{(1 - \theta + \frac{\kappa}{2}\theta)^2} \quad (19)$$

$$H(1 - \kappa) = \begin{cases} 0, & \kappa \geq 1 \\ 1, & 0 \leq \kappa \leq 1 \end{cases} \quad (20)$$

where, D_{s0} is the surface diffusion coefficient when $\theta = 0$, m^2/s . D_{s0} is given as follows [38]:

$$D_s^0 = 8.29 \times 10^{-7} T^{0.5} \exp\left(-\frac{\Delta H_g^{0.8}}{RT}\right) \quad (21)$$

Considering the effect of irreducible water, D_{s0} is revised as follows [39]:

$$D_s^0 = 8.29 \times 10^{-7} T^{0.5} \exp\left(-\frac{\Delta H_w^{0.8}}{RT}\right) \quad (22)$$

where, ΔH_w is the equivalent heat of gas adsorption considering the existence of IW, J/mol, as follows:

$$\Delta H_w = \beta \Delta H_{gw} + (1 - \beta) \Delta H(0) \quad (23)$$

where, $\Delta H(0)$ is the equivalent adsorption heat on the dry pore surface when $\theta = 0$, J/mol; and ΔH_{gw} is the equivalent adsorption heat on the gas-water interface when $\theta = 0$, J/mol.

The flow velocity of gas surface diffusion is as follows:

$$v_s = \frac{1}{\rho} F_s = -\frac{ZRTD_s C_s}{MP^2} \nabla PH(0) \quad (24)$$

The total flow velocity is:

$$\begin{aligned} v &= \left(\frac{r_e^2}{r_m^2}\right) (\varepsilon_v v_v + \varepsilon_k v_k) + \left(1 - \frac{r_e^2}{r_m^2}\right) v_s \\ &= -\left\{\left(\frac{r_e^2}{r_m^2}\right) \left[\frac{\varepsilon_v r_e^2}{8\mu} (1 + \alpha \cdot K_n^*) \left(1 + \frac{4K_n^*}{1 - b \cdot K_n^*}\right) + \frac{\varepsilon_k MD_k}{ZRT}\right] + \left(1 - \frac{r_e^2}{r_m^2}\right) \frac{ZRTD_s C_s}{MP^2}\right\} \nabla P \end{aligned} \quad (25)$$

2.4. Gas Apparent Permeability Model

The calculation equation of gas non-Darcy seepage, as proposed by Javadpour, is as follows:

$$v = -\frac{k_{app}}{\mu} \nabla P \quad (26)$$

By comparing Equation (25) with Equation (26), the equation of apparent permeability can be derived:

$$k_{app} = \left(\frac{r_e^2}{r_m^2}\right) \frac{\varepsilon_r r_e^2}{8} (1 + \alpha \cdot K_n^*) \left(1 + \frac{4K_n^*}{1 - b \cdot K_n^*}\right) + \left(\frac{r_e^2}{r_m^2}\right) \frac{\varepsilon_k \mu MD_k}{ZRT} + \left(1 - \frac{r_e^2}{r_m^2}\right) \frac{\mu ZRTD_s C_s}{MP^2} \quad (27)$$

2.5. Model Verification

To verify the proposed apparent permeability model, we compare the data in our paper with those in [39]. The apparent permeability varying with pressure is shown in Figure 2. As can be seen from Figure 2, the results in this paper closely match the reference sources, indicating the correctness of the model proposed.

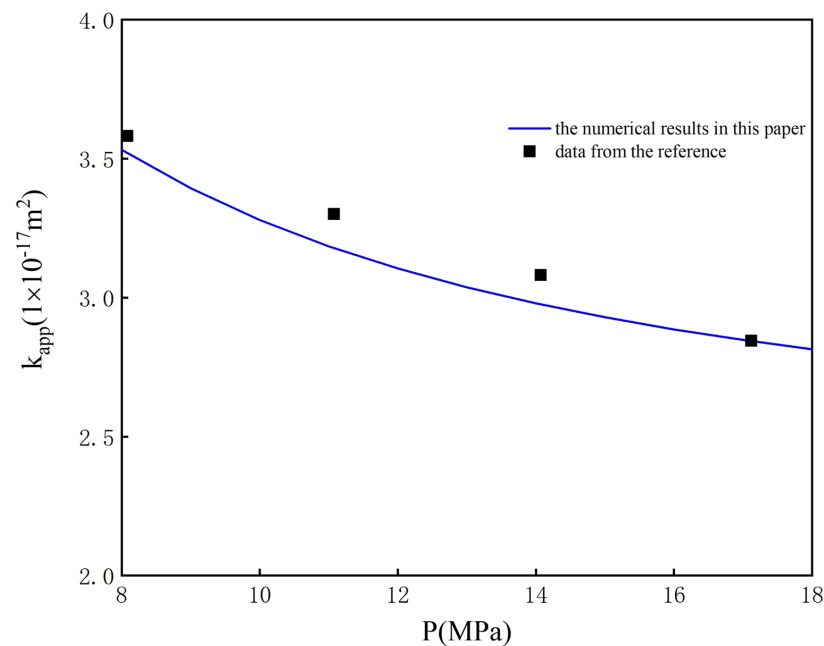


Figure 2. Comparison between the reference results and the numerical results in this paper.

3. Results and Discussion

With the basic parameters of the solution, we can analyze the flow capacity of the k_{app} model, including the effect of K_{np} and the effect of irreducible water (IW). The basic parameters are shown in Table 1.

Table 1. List of basic parameters.

Parameter	Value and Unit	Meaning
d	0.38 nm	Methane molecular diameter
μ	0.0011 mPa·s	Methane gas viscosity
M	Methane gas viscosity	Methane molar mass
S_r	300 m ² /g	Specific surface area of shale
ρ_r	2.8×10^3 kg/m ³	Shale density
d_H	0.4 nm	Water molecular diameter
k_b	1.38×10^{-23} J/K	Boltzmann constant
R	8.314 J/mol/K	Ideal gas constant
P_L	2.1 MPa	Methane Langmuir pressure constant
α	1000	Unit conversion coefficient
ϕ	0.05	Shale porosity
b	-1	Slippage effect fitting constant
N_a	6.02×10^{23}	Avogadro constant
T	310 K	Temperature
P_c	4.539 MPa	Critical pressure of methane
T_c	190.5 K	Critical temperature of methane
$\Delta H_{g/w}$	7953 J/mol	Gas-water interface when gas coverage is 0
$\Delta H(0)$	12,000 J/mol	Equivalent adsorption heat on the dry surface when gas coverage is 0
κ	0.5	Ratio of surface diffusion advance rate to blocking rate
P_H	22.28 MPa	Langmuir pressure constant of methane gas-water interface

3.1. Effect of Knudsen Number Correction

Taking r_m as 10 nm, the variation in apparent permeability under K_n or K_{np} with pressure is calculated, as shown in Figure 3.

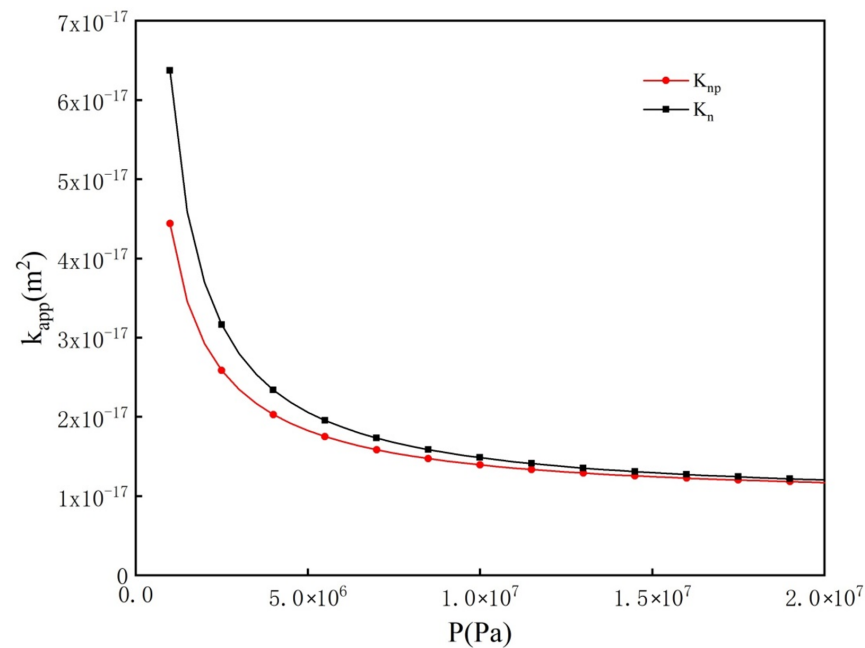


Figure 3. Apparent permeability vs. pressure with K_{np} or K_n ($r_m = 10$ nm).

It can be seen in Figure 3, that the apparent permeability with K_{np} is lower than that with K_n . The effect of K_{np} on the apparent permeability decreases when the pressure increases. After the pressure exceeds 10 MPa, this effect is almost negligible, so the K_n correction can be ignored. However, when the pressure is within 10 MPa, the K_n correction has a certain influence on the actual apparent permeability calculation, so it is necessary to consider the Knudsen correction in this situation. We calculate the change in apparent permeability with pore radius. At the same time, we take different pressures 1 MPa, 5 MPa, 10 MPa for comparative analysis. The result is shown in Figure 4.

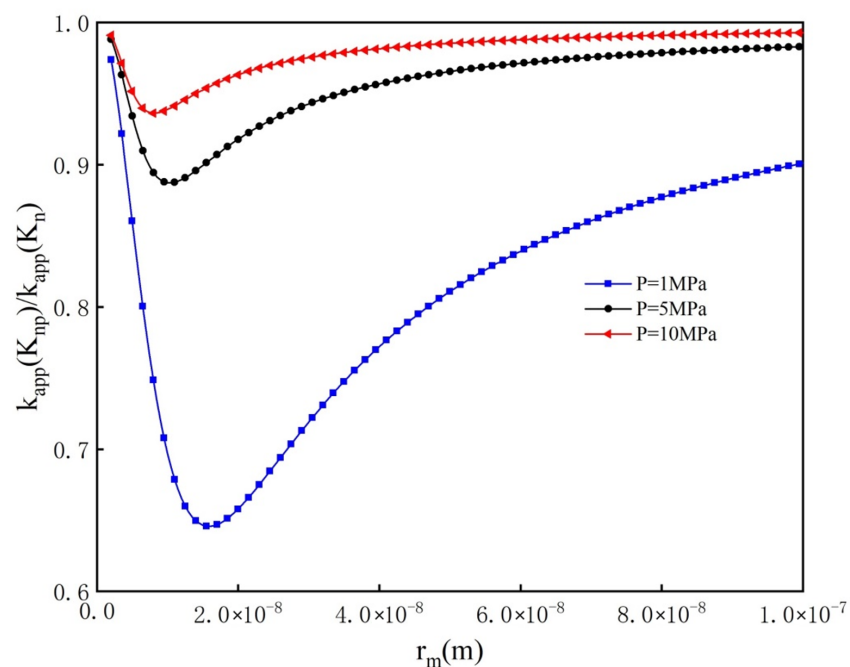


Figure 4. Apparent permeability ratio vs. pore radius with K_{np} or K_n under different pressures.

As seen in Figure 4, under different pressure, with increase in pore radius, the effect of K_{np} on apparent permeability first increases and then decreases, and the final value approaches 1. At the same time, the smaller the pressure is, the greater the peak value of the correction effect is. This is consistent with the earlier conclusion that the effect of the K_n correction is significant when the pressure is small. At the same time, it is noted that the pore radius range of the significant correction is that of medium pores. At medium pore size, about [10nm to 60nm], the effect of the K_n correction needs to be considered.

3.2. Flow Mechanism Analysis

The ratio of flow mechanism is defined as follows:

$$\gamma_1 = \frac{k_b}{k_{app}}; \gamma_2 = \frac{k_s}{k_{app}} \quad (28)$$

where, k_b is the apparent permeability of bulk transport, defined as follows:

$$k_b = k_v + k_k \quad (29)$$

Considering the existence of irreducible water (IW) or not, under 1 MPa and 10 MPa pressure, the extent of flow mechanism with pore radius is analyzed, as shown in Figures 5–8.

The following inferences can be drawn from the above figures:

(1) Under different conditions, the ratio of bulk phase transport to surface diffusion follows the same trend. With increase in the pore radius, the contribution of bulk phase gas transport also increases. With increase in the pore radius, the contribution of surface gas diffusion decreases, which is consistent with the nature of surface diffusion.

(2) Considering the effect of the K_n correction: If the ratio of bulk transport is equal to that of surface diffusion, the point of intersection is called the flow equivalent point. Comparing Figure 5 with Figure 6, and Figure 7 with Figure 8, it can be seen that, compared with considering K_n , the flow equivalent point considering K_{np} moves in the direction of increasing pore radius. This shows that, considering K_{np} , the rising trend in the bulk phase transport proportion and the decreasing trend in the surface diffusion proportion are smaller than those considering K_n . Moreover, bulk phase transport replaces surface diffusion more slowly than when considering K_n .

(3) When the pressure increases, the flow equivalent point moves in the direction of a small pore radius, which indicates that the rising trend in the bulk phase transport proportion, and the decreasing trend in the surface diffusion proportion, under high pressure, are larger than those under low pressure, and bulk phase transport replaces the surface diffusion faster.

(4) Considering the existence of irreducible water (IW), the flow equivalent point moves in the direction of a large pore radius, which indicates that the rising trend in the bulk phase transport proportion and the decreasing trend in the surface diffusion proportion are smaller than those without considering IW, and bulk phase transport replaces surface diffusion more slowly.

3.3. Effect of Irreducible Water

As can be seen from Figures 9 and 10, the gas apparent permeability decreases when the pressure increases. Under different pressure, the apparent permeability with a large β value is always larger than that with a low β value, and the difference under different conditions decreases when the pore radius increases.

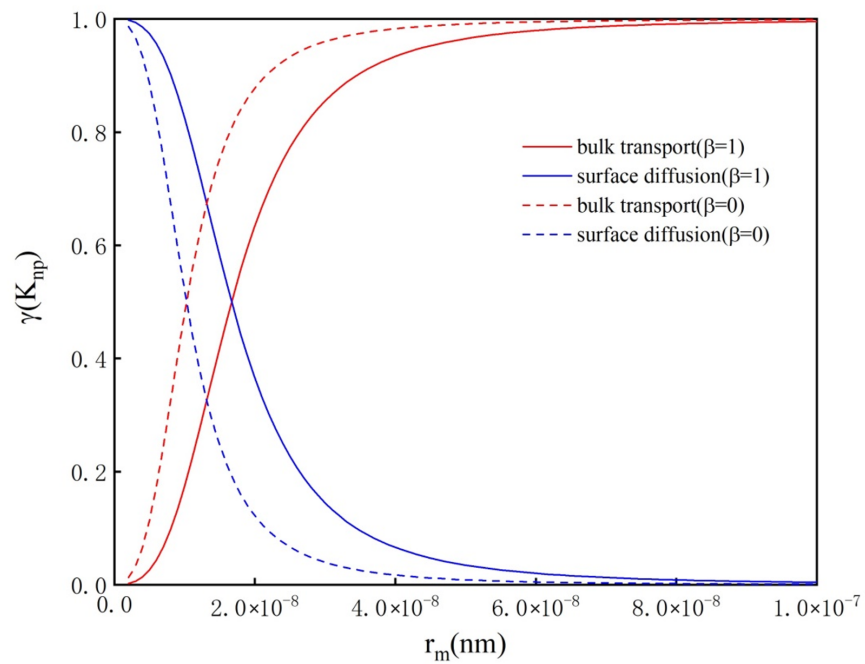


Figure 5. Under different degrees of water molecular coverage, considering K_{np} , the ratio of flow mechanism vs. pore radius ($P = 1$ MPa).

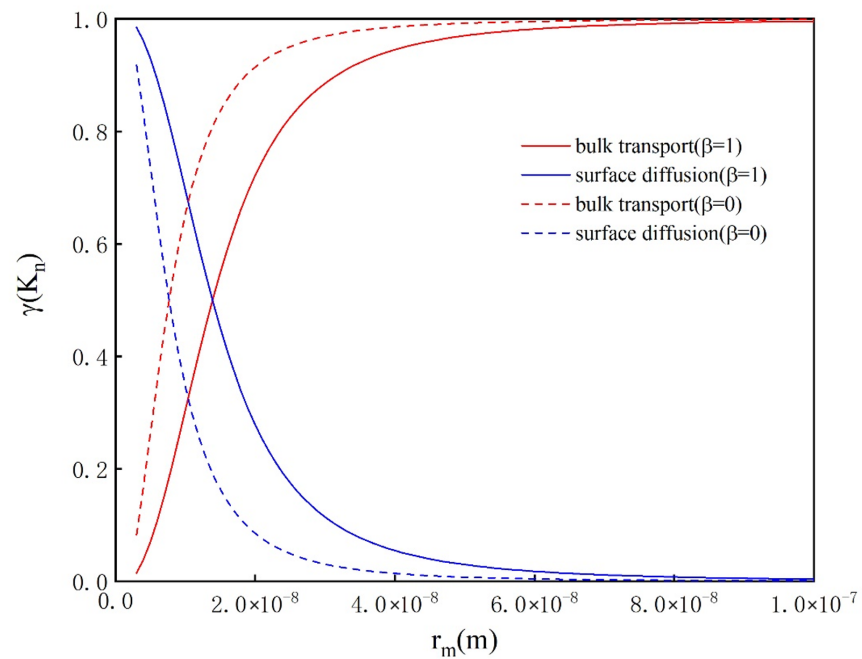


Figure 6. Under different degrees of water molecular coverage, considering K_n , the ratio of flow mechanism vs. pore radius ($P = 1$ MPa).

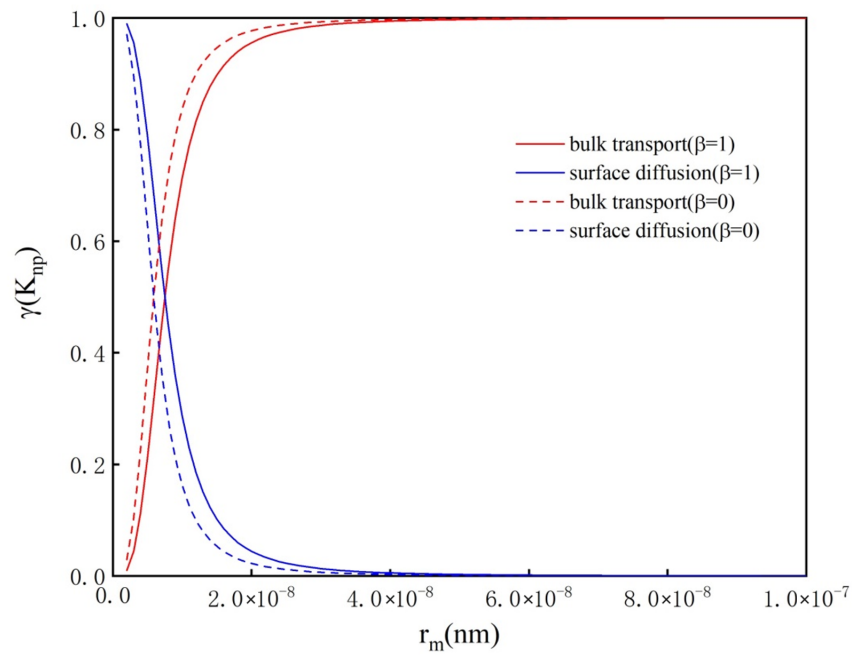


Figure 7. Under different degrees of water molecular coverage, considering K_{np} , the ratio of flow mechanism vs. pore radius ($P = 10$ MPa).

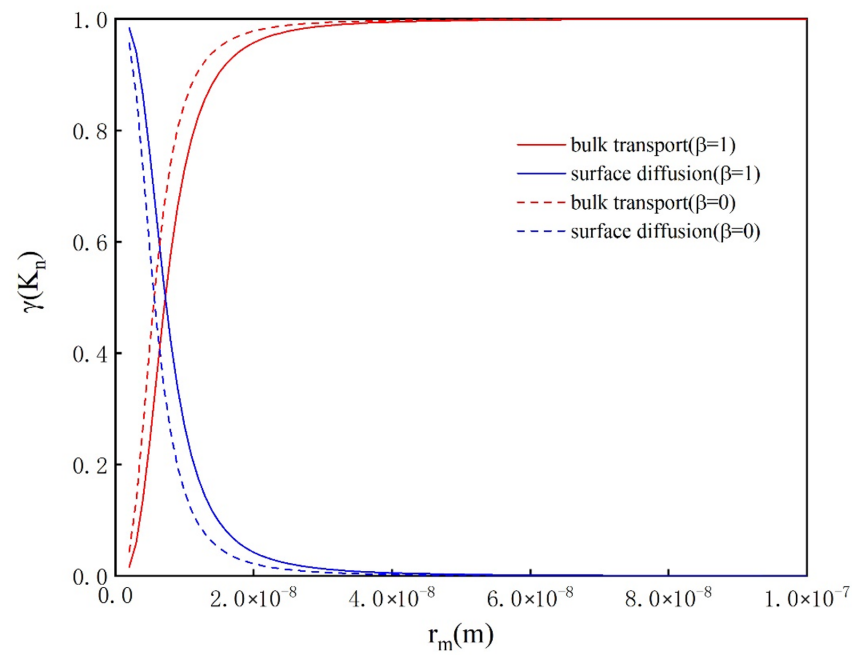


Figure 8. Under different degrees of water molecular coverage, considering K_n , the ratio of flow mechanism vs. pore radius ($P = 10$ MPa).

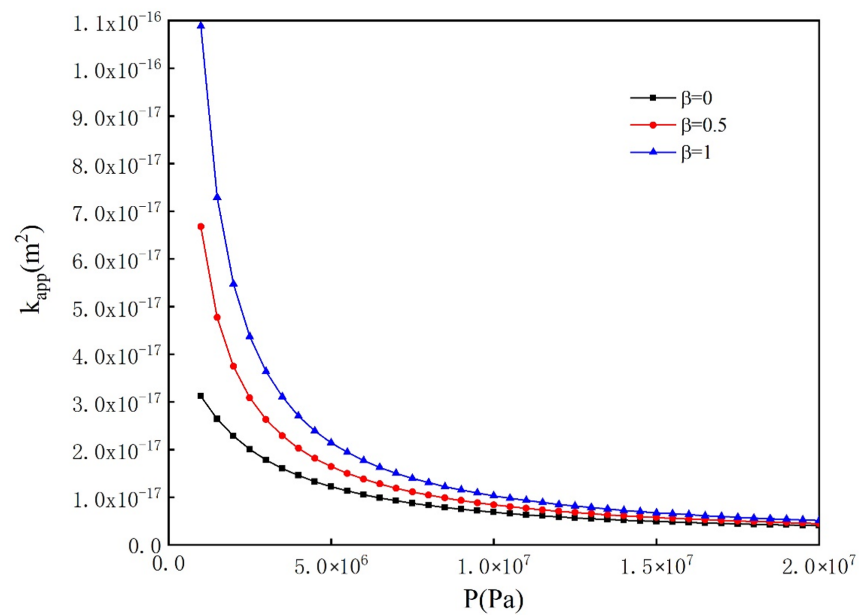


Figure 9. Apparent permeability vs. pressure under different water molecular coverage ($r = 5$ nm).

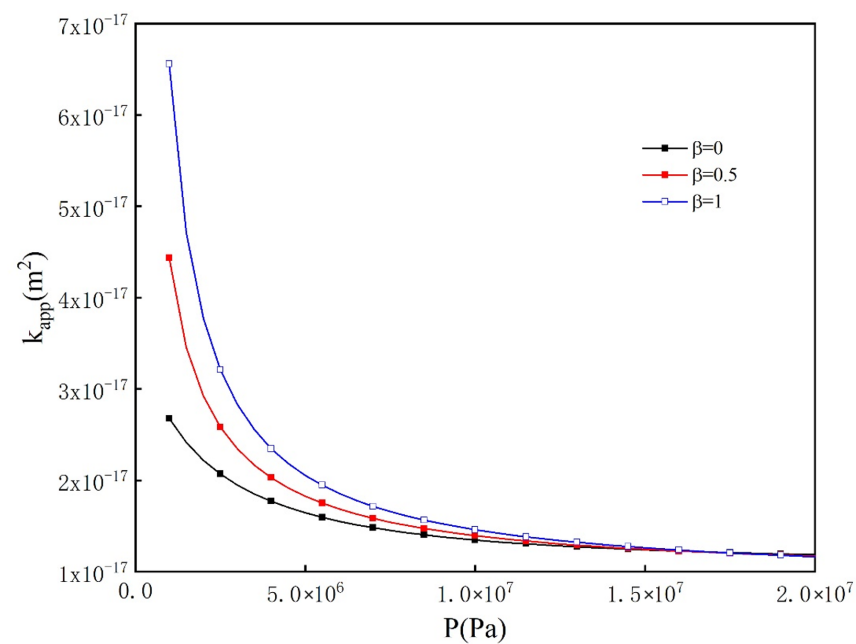


Figure 10. Apparent permeability vs. pressure under different water molecular coverage ($r = 10$ nm).

The characteristic parameter reflecting the effect of IW on gas transport in shale nanopores is defined as follows:

$$\eta = \frac{k_{app}(\beta = 0)}{k_{app}(\beta = 1)} \quad (30)$$

where, η is the ratio of the apparent permeability when the water molecule coverage is 0 to the apparent permeability when the water molecule coverage is 1. If $\eta > 1$, it indicates that the IW effect has a negative influence; that is, the existence of IW can hinder the gas flow

The variation in η with r_m under different pressure is shown in Figure 10.

It can be seen from Figure 11 that, with increase in the pore radius (r), the characteristic parameters gradually increase, and the value is greater than 1, then the characteristic parameters begin to decrease, but the value is still greater than 1. From the definition of the characteristic parameters, we know that the positive influence of IW decreases with increase in r ; that is, in small pores, the effect of bound water is to strongly promote gas flow. In large pores, the positive influence of IW becomes weaker, and can even become negative. With further increase in r , the negative influence begins to decrease, and finally tends to have no effect on the IW.

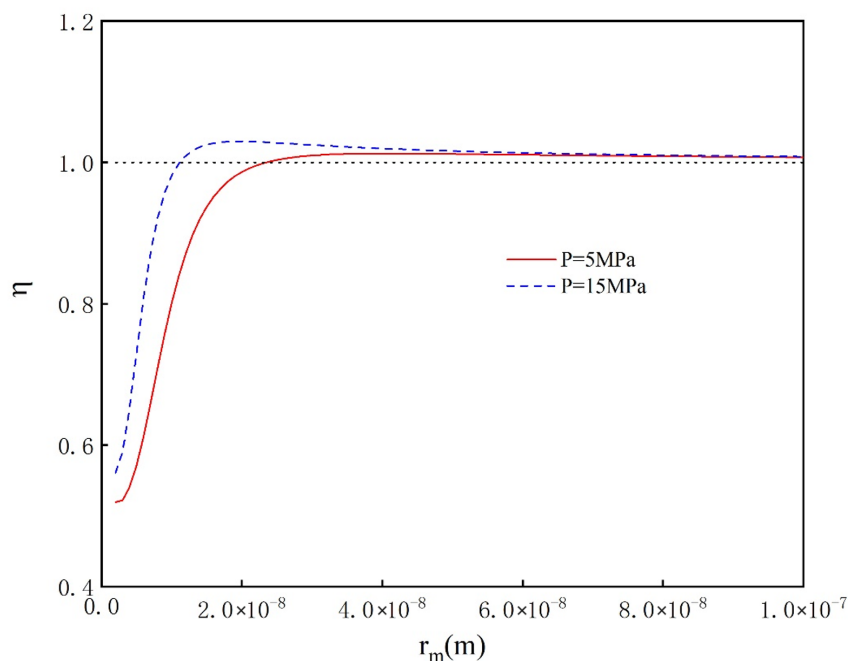


Figure 11. Characteristic parameters vs. pore radius under different pressures.

The effect of IW under low pressure is more obvious than that under high pressure, and the turning point is faster than that under high pressure. Under 5 MPa, the pore radius reaches about 10 nm, and the effect of IW begins to become negative; under 15 MPa, the pore radius reaches about 25 nm, and the effect of IW begins to turn into a negative effect. At the same time, according to the trend of the curve, although the effect of IW can be turned into a negative effect under ultra-high pressure, the negative effect is not obvious because the characteristic parameter of water content is too close to 1. Therefore, under ultra-high pressure, only the positive effect of IW is considered; that is, the effect of IW can promote gas flow under ultra-high pressure.

4. Conclusions

In inorganic pores, there are several flow mechanisms, such as Knudsen diffusion, the slippage effect and surface diffusion. At the same time, due to the existence of irreducible water (IW), the gas percolation process is more complex. The following conclusions are drawn from the study:

(1) Generally speaking, it is necessary to consider the Knudsen number correction in the medium pores (pore radius of about 10 nm to 60 nm) and under low pressure (within 10 MPa). However, under a high pressure and in small or large pores, the Knudsen number correction has a trivial effect on the gas apparent permeability.

(2) The ratio of bulk phase transport increases with increase in the pore radius, while the ratio of surface diffusion decreases with increase in the pore radius. Considering the effect of the Knudsen number correction, bulk phase transport replaces surface diffusion more slowly. Under high pressure, bulk phase transport replaces surface diffusion

faster. Considering the existence of IW, bulk phase transport replaces surface diffusion more slowly.

(3) The effect of IW on the gas apparent permeability decreases with increase in pressure. The existence of IW promotes fluid flow when the pore radius is smaller than the medium pore size (10 nm–60 nm). However, with increase in the pore radius, IW gradually exerts a negative influence on fluid flow. In the case of pressure lower than 0 MPa, the IW, where pore size is small, promotes fluid flow, while the IW, where pore size is large, hinders fluid flow. In the case of ultra-high pressure (larger than 15 MPa), the IW only promotes gas flow.

Author Contributions: Conceptualization, S.Z. and H.L.; methodology, S.Z.; software, C.G. and E.J.; validation, H.L., N.Z. and B.B.; formal analysis, S.Z. and H.L.; writing—original draft preparation, S.Z. and C.G.; writing—review and editing, S.Z. and C.G.; supervision, B.B. All authors have read and agreed to the published version of the manuscript.

Funding: This research was funded by National Natural Science Foundation of China: No. 51704265 and the Outstanding Talent Development Project of the China University of Geosciences (CUG20170614).

Institutional Review Board Statement: Not applicable.

Informed Consent Statement: Not applicable.

Data Availability Statement: Not applicable.

Acknowledgments: The authors acknowledge support from National Natural Science Foundation of China: No. 51704265 and the Outstanding Talent Development Project of the China University of Geosciences (CUG20170614).

Conflicts of Interest: The authors declare no conflict of interest.

References

- Gamou, S.; Yokoyama, R.; Ito, K. Optimal unit sizing of cogeneration systems under the toleration for shortage of energy supply. *Int. J. Energy Res.* **2000**, *24*, 61–75. [\[CrossRef\]](#)
- Li, J.; Li, M.; Li, Y. Strategies Analysis on Energy Shortage and Influence in China. In Proceedings of the 3rd Annual Meeting of Risk-Analysis-Council-of-China-Association-for-Disaster-Prevention, Guangzhou, China, 8–9 November 2008; pp. 729–734.
- Xiao, Z.; Gao, J.; Wang, Z.; Yin, Z.; Xiang, L. Power shortage and firm productivity: Evidence from the World Bank Enterprise Survey. *Energy* **2022**, *247*, 123479. [\[CrossRef\]](#)
- Gong, J.; Qiu, Z.; Zou, C.; Wang, H.; Shi, Z. An integrated assessment system for shale gas resources associated with graptolites and its application. *Appl. Energy* **2020**, *262*, 114524. [\[CrossRef\]](#)
- Tonglou, G. Key geological issues and main controls on accumulation and enrichment of Chinese shale gas. *Pet. Explor. Dev.* **2016**, *43*, 349–359.
- Guo, W.; Liu, H.L.; Xue, H.Q.; Li, X.B. Research and Applications on the Theory of Shale Gas Depth Enrichment Zone. In *Advanced Materials Research*; Trans Tech Publications: Wollerau, Switzerland, 2013; Volume 734, pp. 422–425.
- Xusheng, G.; Dongfeng, H.; Yuping, L.; Zhihong, W.; Xiangfeng, W.; Zhujiang, L. Geological factors controlling shale gas enrichment and high production in Fuling shale gas field. *Pet. Explor. Dev.* **2017**, *44*, 513–523.
- Kok, M.; Mery, S. Shale gas: Current perspectives and future prospects in Turkey and the world. *Energy Sources Part A Recovery Util. Environ. Eff.* **2014**, *36*, 2492–2501. [\[CrossRef\]](#)
- Tang, X.; Jiang, Z.; Song, Y.; Luo, Q.; Li, Z.; Wang, G.; Wang, X. Advances on the mechanism of reservoir forming and gas accumulation of the Longmaxi Formation shale in Sichuan Basin, China. *Energy Fuels* **2021**, *35*, 3972–3988. [\[CrossRef\]](#)
- Xie, J.; Qin, Q.; Fan, C. Influencing Factors of Gas Adsorption Capacity of Marine Organic Shale: A Case Study of Dingshan Area, Southeast Sichuan. *J. Coast. Res.* **2019**, *93*, 507–511. [\[CrossRef\]](#)
- Xue, L.; Chen, B. Exploring on the measurement methods of shale gas content. In Proceedings of the 2016 3rd International Conference on Materials Engineering, Manufacturing Technology and Control, Taiyuan, China, 27–28 February 2016; Atlantis Press: Dordrecht, The Netherlands, 2016; pp. 575–578.
- Haikuan, N.; Jinchuan, Z.; Shengling, J. Types and characteristics of the Lower Silurian shale gas reservoirs in and around the Sichuan Basin. *Acta Geol. Sin.-Engl. Ed.* **2015**, *89*, 1973–1985. [\[CrossRef\]](#)
- Wang, Z. RETRACTED ARTICLE: Characterization of the microscopic pore structure of the lower paleozoic shale gas reservoir in the Southern Sichuan Basin and its influence on gas content. *Pet. Sci. Technol.* **2017**, *35*, 2165–2171. [\[CrossRef\]](#)
- Yao, J.; Song, W.; Li, Y.; Sun, H.; Yang, Y.; Zhang, L. Study on the influence of organic pores on shale gas flow ability. *Sci. Sin. Phys. Mech. Astron.* **2017**, *47*, 094702. [\[CrossRef\]](#)

15. Zhang, J.; Li, X.; Zou, X.; Li, J.; Xie, Z.; Wang, F. Characterization of multi-type pore structure and fractal characteristics of the Dalong Formation marine shale in northern Sichuan Basin. *Energy Sources Part A Recovery Util. Environ. Eff.* **2020**, *42*, 2764–2777. [[CrossRef](#)]
16. Zhang, J.; Li, X.; Xiaoyan, Z.; Zhao, G.; Zhou, B.; Li, J.; Xie, Z.; Wang, F. Characterization of the full-sized pore structure of coal-bearing shales and its effect on shale gas content. *Energy Fuels* **2019**, *33*, 1969–1982. [[CrossRef](#)]
17. Zhang, P.; Hu, L.; Meegoda, J.N. Pore-scale simulation and sensitivity analysis of apparent gas permeability in shale matrix. *Materials* **2017**, *10*, 104. [[CrossRef](#)]
18. Chen, L.; Zuo, L.; Jiang, Z.; Jiang, S.; Liu, K.; Tan, J.; Zhang, L. Mechanisms of shale gas adsorption: Evidence from thermodynamics and kinetics study of methane adsorption on shale. *Chem. Eng. J.* **2019**, *361*, 559–570. [[CrossRef](#)]
19. Beskok, A.; Karniadakis, G.E. Report: A model for flows in channels, pipes, and ducts at micro and nano scales. *Microscale Thermophys. Eng.* **1999**, *3*, 43–77.
20. Javadpour, F. Nanopores and apparent permeability of gas flow in mudrocks (shales and siltstone). *J. Can. Pet. Technol.* **2009**, *48*, 16–21. [[CrossRef](#)]
21. Civan, F. Effective correlation of apparent gas permeability in tight porous media. *Transp. Porous Media* **2010**, *82*, 375–384. [[CrossRef](#)]
22. Xiong, X.; Devegowda, D.; Michel, G.; Sigal, R.F.; Civan, F. A fully-coupled free and adsorptive phase transport model for shale gas reservoirs including non-Darcy flow effects. In Proceedings of the SPE Annual Technical Conference and Exhibition, San Antonio, TX, USA, 8–10 October 2012. [[CrossRef](#)]
23. Darabi, H.; Ettehad, A.; Javadpour, F.; Sepehrnoori, K. Gas flow in ultra-tight shale strata. *J. Fluid Mech.* **2012**, *710*, 641–658. [[CrossRef](#)]
24. Li, J.; Chen, Z.; Wu, K.; Zhang, T.; Zhang, R.; Xu, J.; Li, R.; Qu, S.; Shi, J.; Li, X. Effect of water saturation on gas slippage in circular and angular pores. *AIChE J.* **2018**, *64*, 3529–3541. [[CrossRef](#)]
25. Wu, K.; Chen, Z.; Li, X.; Xu, J.; Li, J.; Wang, K.; Wang, H.; Wang, S.; Dong, X. Flow behavior of gas confined in nanoporous shale at high pressure: Real gas effect. *Fuel* **2017**, *205*, 173–183. [[CrossRef](#)]
26. Wang, J.; Kang, Q.; Wang, Y.; Pawar, R.; Rahman, S.S. Simulation of gas flow in micro-porous media with the regularized lattice Boltzmann method. *Fuel* **2017**, *205*, 232–246. [[CrossRef](#)]
27. Verma, B.; Demsis, A.; Agrawal, A.; Prabhu, S. Semiempirical correlation for the friction factor of gas flowing through smooth microtubes. *J. Vac. Sci. Technol. A Vacuum Surfaces Film.* **2009**, *27*, 584–590. [[CrossRef](#)]
28. Zeng, S.; Hunt, A.; Greif, R. Mean free path and apparent thermal conductivity of a gas in a porous medium. *J. Heat Transf.* **1995**, *117*. [[CrossRef](#)]
29. Li, J.; Li, X.; Wu, K.; Wang, X.; Shi, J.; Yang, L.; Zhang, H.; Sun, Z.; Wang, R.; Feng, D. Water sorption and distribution characteristics in clay and shale: Effect of surface force. *Energy Fuels* **2016**, *30*, 8863–8874. [[CrossRef](#)]
30. Guo, C.; Liu, H.; Xu, L.; Zhou, Q. An improved transport model of shale gas considering three-phase adsorption mechanism in nanopores. *J. Pet. Sci. Eng.* **2019**, *182*, 106291. [[CrossRef](#)]
31. Song, W.; Yao, J.; Li, Y.; Sun, H.; Zhang, L.; Yang, Y.; Zhao, J.; Sui, H. Apparent gas permeability in an organic-rich shale reservoir. *Fuel* **2016**, *181*, 973–984. [[CrossRef](#)]
32. Li, D.; Wang, Y.; Zeng, B.; Lyu, Q.; Zhou, X.; Zhang, N. Optimization of the shale gas reservoir fracture parameters based on the fully coupled gas flow and effective stress model. *Energy Sci. Eng.* **2021**, *9*, 676–693. [[CrossRef](#)]
33. Klinkenberg, L. The permeability of porous media to liquids and gases. *Am. Petrol. Inst. Drill. Prod. Pract.* **1941**, *2*, 200–213. [[CrossRef](#)]
34. Wu, K.; Li, X.; Guo, C.; Wang, C.; Chen, Z. A unified model for gas transfer in nanopores of shale-gas reservoirs: Coupling pore diffusion and surface diffusion. *SPE J.* **2016**, *21*, 1583–1611. [[CrossRef](#)]
35. Kast, W.; Hohenthanner, C.R. Mass transfer within the gas-phase of porous media. *Int. J. Heat Mass Transf.* **2000**, *43*, 807–823. [[CrossRef](#)]
36. Krishna, R.; Wesselingh, J. The Maxwell-Stefan approach to mass transfer. *Chem. Eng. Sci.* **1997**, *52*, 861–911. [[CrossRef](#)]
37. Chen, Y.; Yang, R.T. Surface and mesoporous diffusion with multilayer adsorption. *Carbon* **1998**, *36*, 1525–1537. [[CrossRef](#)]
38. Guo, L.; Peng, X.; Wu, Z. Dynamical characteristics of methane adsorption on monolith nanometer activated carbon. *J. Chem. Ind. Eng.* **2008**, *59*, 2726–2732.
39. Bai, J.; Kang, Y.; Chen, M.; Li, X.; You, L.; Chen, Z.; Fang, D. Impact of water film on methane surface diffusion in gas shale organic nanopores. *J. Pet. Sci. Eng.* **2021**, *196*, 108045. [[CrossRef](#)]